Design of stable Ni/ZrO_2 catalysts for dry reforming of methane

Yu Lou[a], Matthias Steib[a], Qi Zhang[b], Konrad Tiefenbacher[b], Anita Horváth[c], Andreas Jentys[a], Yue Liu[a,*], and Johannes A. Lercher[a,*]

[a]Department of Chemistry and Catalysis Research Center, TU München, Lichtenbergstr. 4, 85748 Garching (Germany)

[b]Department of Chemistry, University of Basel, St. Johanns-Ring 19, CH-4056 Basel, Switzerland; Department of Biosys-tems Science and Engineering, ETH Zürich, Mattenstrasse 26, CH-4058 Basel, Switzerland

[c]Institute for Energy Security and Environmental Safety, Centre for Energy Research, Konkoly-Thege M. street 29-33, H-1121 Budapest, Hungary

* Corresponding author.
Email: yue.liu@tum.de (Y. Liu),
johannes.lercher@tum.de (J. A. Lercher)

Abstract

ZrO_2 supported Ni with an average particle diameter of 1-2 nm were synthesized by binding Ni^{2+} in rccc-5,11,17,23-tetrahydroxy-2,8,14,20-tetra(n-ndecyl)resorc[4]arene (pyrogallol[4]arene) nano-capsules as Ni precursor. The Ni/ZrO_2 catalyst with a 1.1 nm particle diameter showed outstanding stability in dry reforming of methane (DRM), which maintained nearly 90% of the initial activity after 60 h time on stream. The high stability is attributed to nearly all Ni atoms being located at the interface and perimeter to ZrO_2. This led to a higher accessibility to the oxygen from activated CO_2 at the Ni-ZrO_2 interface, facilitating conversion of surface carbon to CO. Ni/ZrO_2 catalysts with larger Ni particle diameter have a fraction of non-perimeter Ni that deactivates rapidly. The decrease of the H_2 formation rate was faster with time on stream than the decrease of the H_2O formation rate. At longer time on stream the ratio of H_2O to H_2 yield reached 0.40 ± 0.08 for all Ni/ZrO_2 catalysts, independently if a catalyst was stable from the reaction start or deactivated to a stable level. The ratio between H_2O and H_2 yield reflects the abundance of oxygen availability on the Ni surface, the oxygen availability index (OAI). For an OAI value of 0.40, the deactivation of Ni catalyst was negligible, while below that deactivation was pronounced. The reorganization of surface carbon to graphitic overlayers and carbon fibers is hypothesized to start from surface domains that are not adjacent to the metal-support perimeter.

Keywords: dry reforming of methane; nickel; nanocapsule; deactivation; perimeter

Introduction

The ability to utilize small-scale gas fields (shale gas) and the coexisting impurities of CO_2 has renewed the interest in dry reforming (Eq. 1). The high C/O ratio of dry reforming makes carbon formation, not only thermodynamically very favorable, but frequently leads to excessive carbon deposition, and reactor blocking [1].

$$CO_{2(g)} + CH_{4(g)} \rightleftharpoons 2\ CO_{(g)} + 2\ H_{2(g)} \quad (1)$$

Typical catalysts, kinetically limiting carbon formation, include VIIIA metals as well as noble metals on refractory oxide supports. On these catalysts, side reactions occur including reverse water gas shift (Eq. 2), methane cracking (Eq. 3) and the Boudouard reaction (Eq. 4) depositing carbon on the catalyst. Especially on supported VIIIA metals catalysts such as Ni, severe coke formation leads to a strong deactivation [1, 2].

$$CO_{2(g)} + H_{2(g)} \rightleftharpoons CO_{(g)} + H_2O_{(g)} \quad (2)$$

$$CH_{4(g)} \rightleftharpoons C_{(s)} + 2\ H_{2(g)} \quad (3)$$

$$2\ CO_{(g)} \rightleftharpoons C_{(s)} + CO_{2(g)} \quad (4)$$

Reducing coke formation requires lower rates of methane cracking and of the Boudouard reaction during dry reforming. Empirically, this has been achieved by reducing the metal particle size below a critical Ni particle size ($d < 2$ nm) [3] or via a support with a higher carbon removal ability [4-11]. However, both methane cracking and Boudouard reactions cannot be completely avoided, because they are kinetically coupled with dry reforming through sharing the same species in the elementary step on the metal surface (Table 1).

An alternative strategy is to reduce carbon buildup on the metal by providing kinetically higher concentration of labile oxygen that helps to remove carbon species by oxidation. Recently, the use of oxophilic metals has been proposed for this purpose. With this strategy, the metal component such as Co [12] or Fe [13] is added to the metal primarily active in methane dissociation, e.g., Ni, in order to provide an oxygen reservoir that can be used to oxidize surface carbon. While this is an approach based on thermodynamics, it is conceptually also possible to provide labile oxygen in the reducing atmosphere of the reforming reactor by activating and dissociating CO_2 at the boundary between the perimeter of the metal particles and the support [14].

Table 1 summarizes the main surface elementary reactions during dry reforming. The dissociative chemisorption of CH_4 on the active metal surface denotes the initial step, providing H and C on to the surface (Eq. 5) [15]. The CO_2 molecule is adsorbed and activated on the metal and on the support (Eq. 2) [5, 6, 16, 17], releasing active surface O. Hydrogen atoms leave the surface via two pathways, i.e., two H combining as H_2 (Eq. 7) or reacting with an O as H_2O (Eq. 8). The formation of H_2O decreases the H_2/CO ratio in the product composition. Carbon atoms leave the surface by reacting with O, forming CO (Eq. 9). The imbalance between the C generation at the surface (Eq. 5) and its removal from the surface (Eq. 9) leads to retention of a part of C, which reorganizes, forming coke and blocking active site (Eq. 10). Thus, an efficient supply of active O atoms onto the catalyst surface will increase the rate of C atoms forming CO and desorbing. Reducing the concentration and residence time of C on Ni will reduce C reorganization and reduce the formation of graphite overlayers and whiskers.

Table 1. Surface elementary reactions on DRM catalyst.

Description	Elementary reaction	Rate constant	Reaction number
C and H input via CH_4 activation	$CH_4 + 2\ * \rightarrow CH_3* + H*$	k_{5a}	5
	$CH_3* + * \rightarrow CH_2* + H*$	k_{5b}	
	$CH_2* + * \rightarrow CH* + H*$	k_{5c}	
	$CH* + * \rightarrow C* + H*$	k_{5d}	
O input via CO_2 activation	$CO_2 + * \rightleftharpoons CO + O*$	k_{6f}, k_{6r}	6
H output as H_2 and H_2O	$H* + H* \rightleftharpoons H_2 + 2\ *$	K_7	7
	$H* + O* \rightleftharpoons OH* + *$	K_{8a}	8
	$OH* + H* \rightleftharpoons H_2O + 2\ *$	K_{8b}	
C output as CO	$C* + O* \rightarrow CO$	k_9	9
C retaining as coke	$n\ C* \rightarrow Coke^{n}*$	k_{10}	10

Oxygen atoms to form CO on the catalyst are supplied by activating and dissociating CO_2. Two reaction pathways have been identified for this step. On the metal surface, CO_2 is dissociated into adsorbed CO and O. In addition, at the boundary between the metal particle perimeter and the support a second and more efficient pathway to activate CO_2 in the form of carbonate takes place, allowing to transfer an O atom to the perimeter metal atoms. The utilization of transition metal oxides that have the ability to form carbonates as well as having

oxygen storage capacity, i.e., ZrO_2 [3-6, 16-19] and CeO_2 [7-9, 20], has been extensively investigated. The transfer of these labile oxygen atoms to increase the abundance of O atom on the metal will occur at the metal-support interface. Maximizing the kinetic availability of labile oxygen requires, therefore, maximizing the fraction of perimeter metal atoms. Obviously, the synthesis of small metal particles on suitable supports is the most straightforward strategy to achieve this.

In order to prepare small metal nanoparticles for DRM, especially for base metals such as Ni, several efforts [10, 21-27] have been reported, confining the metal or its precursors in well-defined structures, including inorganic frameworks [28-34] and organic colloids [21]. Catalysts with Ni particle size as small as 2 nm were successfully prepared in this way [21, 35]. These methods, however, require challenging synthesis procedures and rigorous preparation conditions during the synthesis.

We report here a new robust approach to synthesize 1 nm Ni nanoparticles supported on ZrO_2 and SiO_2 by using air-stable Ni colloids, consisting of Ni^{2+} binding in nanocapsules from the self-assembly of rccc-5,11,17,23-tetrahydroxy-2,8,14,20-tetra(n-ndecyl)resorc[4]arene (pyrogallol[4]arene) [36-44], to limit Ni sintering during initial formation at high temperature. We will show that these resulting particles not only have a unique stability, but also helped to define a final state of stable reforming catalysts.

Experimental

General. All chemicals were obtained from commercial suppliers and used as received. Ni(II) nitrate hexahydrate (Sigma–Aldrich, ≥ 98.5%), zirconium hydroxide (Mel chemicals, XZO1501/03), silicon dioxide (Evonik, Aerosil 200), chloroform ($CHCl_3$) solution (Sigma, ≥ 99.9 %)

Catalyst preparation. Zirconium hydroxide ($Zr(OH)_4$) was calcined in air (flow rate 30 ml·min^{-1}) at 1073 K for 15 h with a heating rate of 0.5 K·min^{-1}. H_2O saturated $CHCl_3$ solution was prepared by dropping H_2O into $CHCl_3$ and mixed by sonication as described previously [43]. Pyrogallol[4]arene was added into the organic phase, forming a clear solution after gentle heating. Subsequently, $Ni(NO_3)_2{\cdot}6H_2O$ was added to the host molecule solution and the solution was stirred overnight until all $Ni(NO_3)_2{\cdot}6H_2O$ was dissolved. After a period of 20 h, the oxide support was added to the nickel colloidal solution before evaporation under reduced

pressure. The as-prepared catalyst was dried at 373 K for 12 h, air-calcined at 673 K (heating rate 0.5 K·min^{-1}) for 2 h (flow rate 100 mL·min^{-1}) and reduced in pure H_2 at 873 K (heating rate 0.5 K·min^{-1}) for 2 h (flow rate 100 mL·min^{-1}).

Catalyst testing. DRM reactions were carried out in a fixed bed reactor. Typically, 50 mg of catalysts (500-710 μm) were diluted with 450 mg SiC (500-710 μm). The catalyst sample was loaded in a quartz reactor (7 mm inner diameter) and reduced with 20 vol% H_2 in N_2 (total flow rate 100 mL·min^{-1}) at 873 K for 2 h before DRM. Afterwards, 25 vol% CH_4 (99.995 vol%), 25 vol% CO_2 (99.995 vol%) and 50 vol% N_2 (99.999 vol%) with a total flow of 100 mL·min^{-1} were introduced into the reactor and the DRM reaction was carried out at the same temperature and atmospheric pressure. N_2 was used as calibration standards. The amount of reaction products were determined online by Shimadzu GC-MS and GC, using TCD and FID as detector.

Reaction rate. The DRM reaction rate r was expressed as methane consumption rate and calculated using the following equations:

$$r = \frac{X_{CH_4} \times F_{CH_4\,in}}{n_{Ni}} \quad (11)$$

in which $F_{CH_4\,in}$ is the CH_4 flow rate in feed gas, n_{Ni} is total amount of Ni on the catalysts and X_{CH_4} is the conversion of CH_4 during DRM reaction using following equation:

$$X_{CH_4} = 1 - \frac{P_{CH_4\,out}}{P_{CH_4\,in}} \times \frac{P_{N_2\,in}}{P_{N_2\,out}} \times 100\% \quad (12)$$

in which $P_{CH_4\,in}$ and $P_{CH_4\,out}$ are the CH_4 pressure in inlet and outlet gas. The conversion of methane was normalized to the partial pressure of N_2 in feed gas ($P_{N_2\,in}$) and outlet gas ($P_{N_2\,out}$) in order to account the effect of volume expansion during the reaction.

Measured reaction rate was corrected for the approach to equilibrium (μ) to forward reaction rate (r_f) based on following Equations.

$$r_f = \frac{r}{1-\mu} \quad (13a)$$

$$\mu = \frac{P_{CO}{}^2 P_{H_2}{}^2}{P_{CH_4} P_{CO_2}} \times \frac{1}{K} \quad (13b)$$

in which P_i is the pressure of *i* species in the gas phase and *K* is equilibrium constants for DRM reaction.

Equipment

AAS. The elemental composition of Ni was measured by atomic absorption spectroscopy (AAS) on a UNICAM 939 AA-Spectrometer. Ethanol was added to the capsule solutions to destruct the host molecules and Ni species was extracted with water before AAS measurement.

XAS. The particle size and oxidation state of Ni species were determined by X-ray absorption measurements at the Super XAS beamline at the SLS in Villigen, Switzerland recorded with a channel-cut Si(111) monochromator [45] with an oscillation frequency of 2 Hz. To get a sufficient signal to noise ratio, spectra were recorded for 5 minutes and merged afterwards. The experiments were carried out *in situ* in a quartz glass capillary (Hilgenberg, 1 mm diameter, 10 µm wall thickness). The flow of the gasses during the experiment was kept constant at 20 $mL \cdot min^{-1}$. After installing a sample, the capillary was flushed for 15 minutes to ensure inert conditions. For in situ reduction of the calcined sample, a hot air blower (FMB Oxford) was used to heat the sample in the capillary with a heating rate of 10 $K \cdot min^{-1}$ to 873 K. After reaching 873 K, the temperature was kept constant for 90 minutes followed by cooling to room temperature. Data analysis was carried out with Athena and Artemis software from the IFEFFIT [46] package and with FEFF6 [47].

*TGA***.** The amount of coke deposits on spent catalysts were quantified by thermogravimetric analysis (TGA) on a SETARAM Sensys Evo system. For these experiments, the reaction was stopped after each step and the catalysts were cooled down in N_2. Typically 10 mg of spent catalysts (SiC free) were loaded in the sample holder. The samples were pretreated in He (flow rate 16 $mL \cdot min^{-1}$) at 473 K (heating rate 10 $K \cdot min^{-1}$) to remove adsorbed H_2O and CO_2 before cooling to 303 K. Subsequently, the temperature was increased to 1073 K (heating rate 5 $K \cdot min^{-1}$) in air (flow rate 16 $mL \cdot min^{-1}$) and kept for 0.5 h. The amount of coke was obtained from the weight loss of the spent catalysts and subtracting the weight increase induced by oxidation of Ni during TGA process.

^{1}H-NMR. The ^{1}H-NMR spectra were recorded at 298 K with a Bruker AV 500 spectrometer using the Bruker standard routine program. The nickel colloidal solution was dissolved in non-deuterated chloroform (0.50 mL). Deuterated dimethyl sulfoxide (DMSO-d_6, 0.15 mL) was added in a coaxial insert tube (Sigma Aldrich) for the field/frequency lock.

Results and discussion

Estimation of particle size threshold for stable Ni/ZrO_2 reforming catalysts.

The fraction of perimeter Ni surface atoms as a function of Ni nanoparticle size was estimated using both half-cuboctahedral and full-cuboctahedral models for Ni nanoparticles on ZrO_2. We have shown previously that CO_2 activated at the oxygen vacancies at the interface between Ni and ZrO_2 forms labile oxygen species in the form of transient carbonates (Fig. 1a) [5, 6, 16-18]. These oxygen atoms are bound to one Ni atom at the interface and can react with either H or C bound to adjacent Ni atoms. Therefore, the Ni atoms at the interface and directly neighboring it are easily accessible to oxygen generated from CO_2. Both are considered, therefore, as perimeter Ni. Consequently, for a Ni half-cuboctahedral nanoparticle with size below 1 nm, only two layers of Ni are present that have all the Ni atoms at this perimeter (Fig. 1a). A third and more layers exist on larger Ni half-cuboctahedral particles, making these Ni atoms less accessible to oxygen (Fig. 1b). Therefore, we hypothesize that the fraction of Ni at the perimeter remains one for the Ni hemi-cuboctahedral particles with a diameter below 1 nm. Above this size threshold this fraction decreases sharply with growing particle size (Fig. 1c, green line). The same trend is seen when cuboctahedral particles are used (Fig. 1c, orange line), but the fraction of perimeter Ni is lower than using half-cuboctahedral model. The above calculations show that an ideal Ni/ZrO_2 catalyst for DRM must have Ni particles below 1 nm on which every Ni is at the perimeter interface on a half-cuboctahedral particle and more than 75% at the perimeter interface on a cuboctahedral particle. CO_2 activation and active O atom supply are fast in that situation to react surface C into CO, leading to a low C concentration and residence time on Ni during DRM.

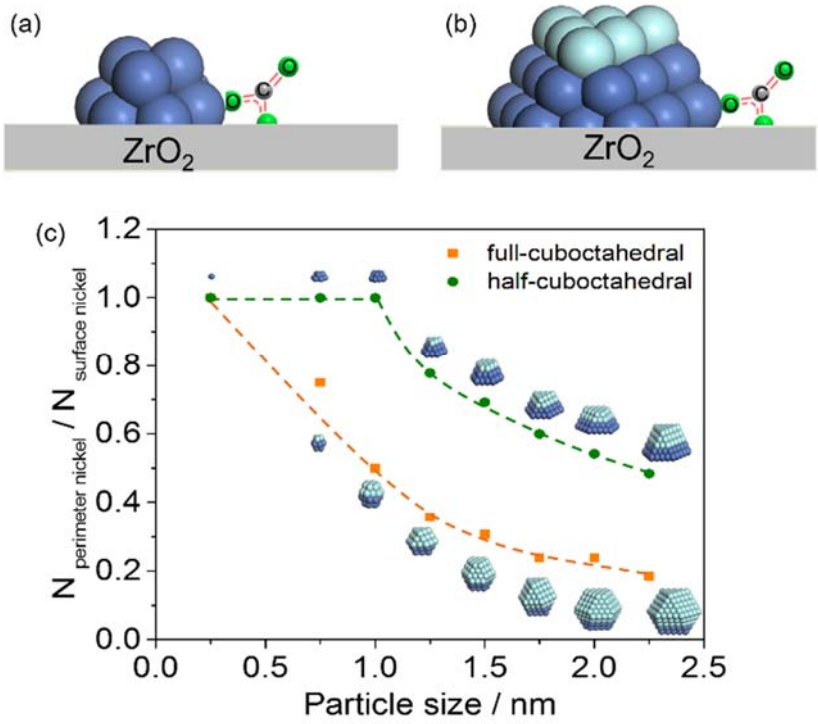

Figure 1. Schematic representation of the carbonate formation in the vicinity of Ni and ZrO_2 over DRM catalysts with metal particle size of 0.75 nm (a) and 1.25 nm (b). (c) Influence of particle size on the fractions of perimeter nickel in total number of surface nickel. The blue balls represent the perimeter Ni atoms and the light blue balls represent the non-perimeter Ni atoms.

Catalyst synthesis and characterization.

To synthesize nano-sized nickel particles on oxide supports, a synthesis method using Ni^{2+} constrained in an organic nanocapsules, pyrogallol[4]arene, was applied. The synthesis strategy is shown in Figure 2. The pyrogallol[4]arene was synthesized according to a literature procedure [48, 49], its structure was confirmed by NMR spectroscopy (see SI). The Ni colloid was prepared by adding $Ni(NO_3)_2{\cdot}6H_2O$ into a water saturated chloroform ($CHCl_3$) solution (Sigma, ≥ 99.9 %) and mixing by sonication as described in detail previously [43]. After 1 h the solution was added to pyrogallol[4]arene yielding a clear solution after gentle heating. The formation of homogeneous nickel supramolecular assemblies prevents aggregation and assures a good dispersion of Ni^{2+} in the precursor solution. The binding of the Ni^{2+} ions by the capsules was confirmed by the dissolution of $Ni(NO_3)_2{\cdot}6H_2O$, which was only slightly soluble without capsule molecules (Fig. 2 and Table 2). By increasing the loading of $Ni(NO_3)_2{\cdot}6H_2O$, the concentration of Ni species in the hexameric pyrogallol[4]arene solution increased from 71 mg/L to 365 mg/L (Table 2), while the nickel concentration did not change in the absence of

pyrogallol[4]arene. This result indicated the transfer of Ni species from solid state to organic solution. The bound Ni species were concluded to be located on the surface of the capsule molecules evidenced by further ^{1}H NMR analysis (Fig. S1 and Table S1), which inserted into the hydrogen-bonding networks by the formation of Ni-O bonds [38, 40].

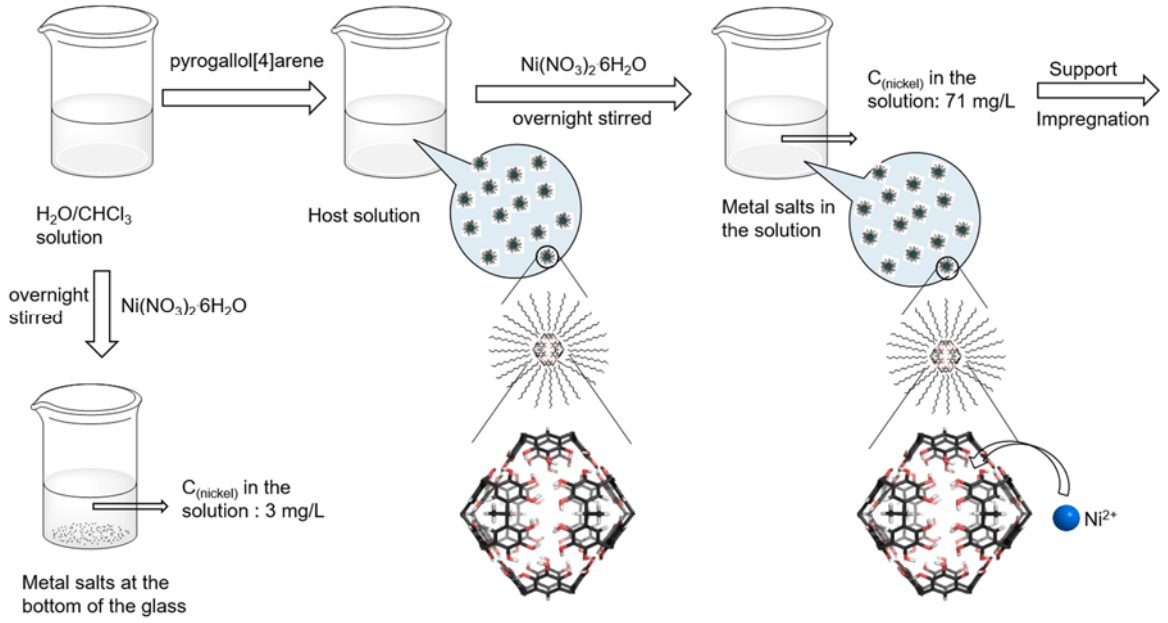

Figure 2. Binding of Ni^{2+} during synthesis procedure with hexameric pyrogallol[4]arene capsule.

Determination of Ni particle size on ZrO_2 was difficult by the conventional methods, i.e., XRD, TEM and XAFS, due to the impact of the ZrO_2 support [11, 50, 51]. Therefore, SiO_2 supported Ni catalysts were used as models for estimating the Ni particle size using XAS. Figure 3 shows the XANES spectra of dried, calcined and reduced 1 wt% Ni/SiO_2 at the Ni K-edge (Fig. 3). The shape of the white line at *ca.* 8350 eV confirmed the presence of oxidized Ni on the dried and in situ calcined samples. After reduction with H_2 at 873 K for 90 minutes, Ni was fully reduced, confirmed by the shift of the absorption edge to 8333 eV in the XANES of Ni (Fig. 3).

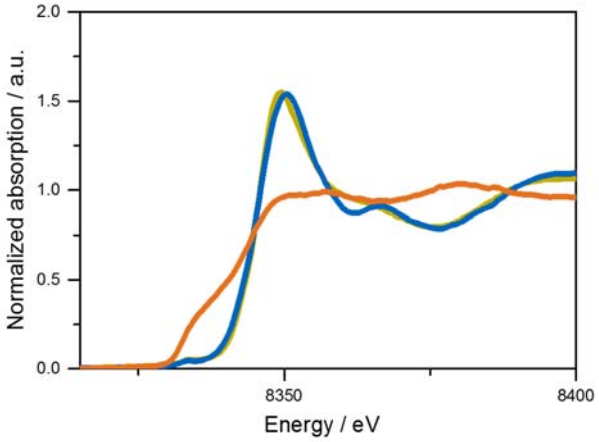

Figure 3. XANES at the Ni K-edge of uncalcined (green), in situ calcined (blue) and in situ reduced (orange) 1 wt.% Ni/SiO_2.

Table 2. Properties of Ni^{2+} precursor solution and the resulting prepared Ni/ZrO_2 catalysts.

Ni^{2+} precursor solution	Ni^{2+} loading into solvent (mg/L)	90	180	450
	Dissolved Ni^{2+} in absence of capsule (mg/L)	3.3	3.3	3.4
	Dissolved Ni^{2+} in presence of capsule (mg/L)	71	150	365
	(nNi^{2+} : ncapsule cage)	(1:1)	(2:1)	(5:1)
Prepared Ni/ZrO_2 samples	Ni loading	1 wt.%	2 wt.%	5 wt.%
	Ni particle size (nm)[a]	1.1	1.5	1.9
	Ni dispersion[b]	68%	50%	39%
	Surface Ni concentration (µmol/g)	117	172	336

a Estimated by EXAFS of corresponding Ni/SiO_2 with same Ni loading amount;
b Calculated from Ni particle size.

The analysis of the EXAFS (Fig. 4 and Table S2) showed the presence of Ni-O contributions and the absence of a metallic Ni environment in the dried uncalcined sample, which is in agreement with the formation of a Ni - organic nanocapsule via Ni-O coordinative bonds. After reduction an average coordination numbers for Ni-Ni of 5.5 was observed for Ni/SiO_2, which indicates the presence of Ni particles with an average particle size of 1.1 nm (Table 2) [52]. Long alkyl chains on the outer surface of these capsules provide the spacer distances between each capsule and metal species and, thus, prevent facile metal-to-metal contact. This reduces the tendency for sintering during calcination [21, 53] and led to small metal particles after high temperature treatment.

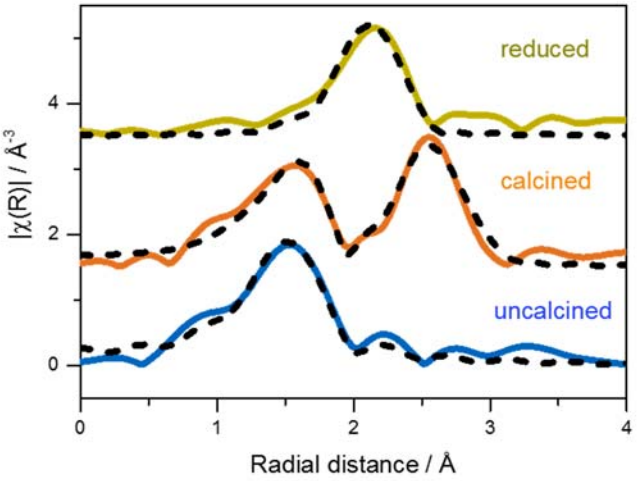

Figure 4. Fourier transformed EXAFS at the Ni K-edge recorded for 1 wt.% Ni/SiO_2 uncalcined (blue line), in situ calcined (orange line) and in situ reduction (green line). The dotted lines are the results of the EXAFS fits.

To explore the influence of Ni loading on the final particle size, EXAFS of 1 wt.%, 2 wt.% and 5 wt.% Ni/SiO_2 after drying and in situ reduction were analyzed (Figure 5 and Table S3). For the dried uncalcined samples, Ni was present in oxidized form (as discussed from the XANES) with the same coordination number (~4.7) for the three samples. After in situ reduction, the disappearance of the Ni-O contributions and a contraction of the Ni-Ni distances were observed. The 1 wt.% Ni/SiO_2 showed the lowest Ni-Ni coordination number of 5.5 within these three catalysts; coordination numbers of 2 wt.% Ni/SiO_2 and 5 wt.% Ni/SiO_2 were 8.6 and 9.7, respectively. Based on these coordination numbers, Ni particle diameters of the 2 wt.% and 5 wt.% Ni/SiO_2 were 1.5 and 1.9 nm, respectively (Table 2). The increasing particle size with the increasing number of Ni^{2+} per nanocapsule demonstrates that the concentration of Ni in the nanocapsule and the proximity of Ni during reduction determines the size of the final supported Ni particle.

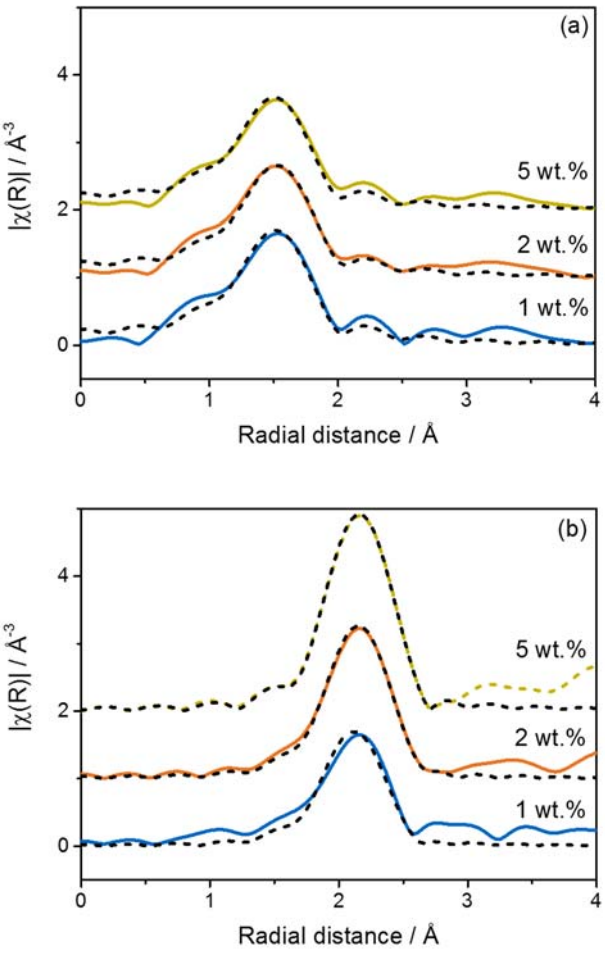

Figure 5. Fourier transformed EXAFS at the Ni K-edge recorded at room temperature of (a) uncalcined and (b) reduced 1 wt.% Ni/ Ni/SiO_2 (blue line), 2 wt.% Ni/SiO_2 (orange line) and 5 wt.% Ni/ Ni/SiO_2 (green line). The dotted lines are the results of the EXAFS fits.

Catalytic performance in DRM.

The catalytic activities of the ZrO_2 and SiO_2 supported Ni catalysts for methane dry reforming are shown as the conversion rate of CH_4 in Figure 6. All the three Ni/ZrO_2 catalysts showed comparable initial methane conversion rate per surface Ni, (1.19 ± 0.04) mol_{CH4} s^{-1} $mol_{surf\ Ni}^{-1}$, regardless of the Ni dispersion and the percentage of perimeter and non-perimeter Ni. This indicates that the perimeter Ni and non-perimeter Ni has the same activity in CH_4 conversion. The Ni/SiO_2 catalyst was the least active, with an initial rate of 0.26 mol_{CH4} s^{-1} $mol_{surf\ Ni}^{-1}$. However, 1 wt.% Ni/ZrO_2 was much more stable against deactivation compared to other catalysts. During the first 500 minutes of reaction the 1 wt.% Ni/ZrO_2 catalyst showed only a slight deactivation, followed by a period of 2500 mins with constant activity. In contrast, the 2 wt.% and 5 wt.% Ni/ZrO_2 experienced fast and continuous deactivation during DRM, which led to a loss of activity of 72 % and 75 % after 900 minutes, respectively. The 1 wt.%

Ni/SiO_2 showed the strongest deactivation, which led to an almost complete loss of activity after 50 min TOS.

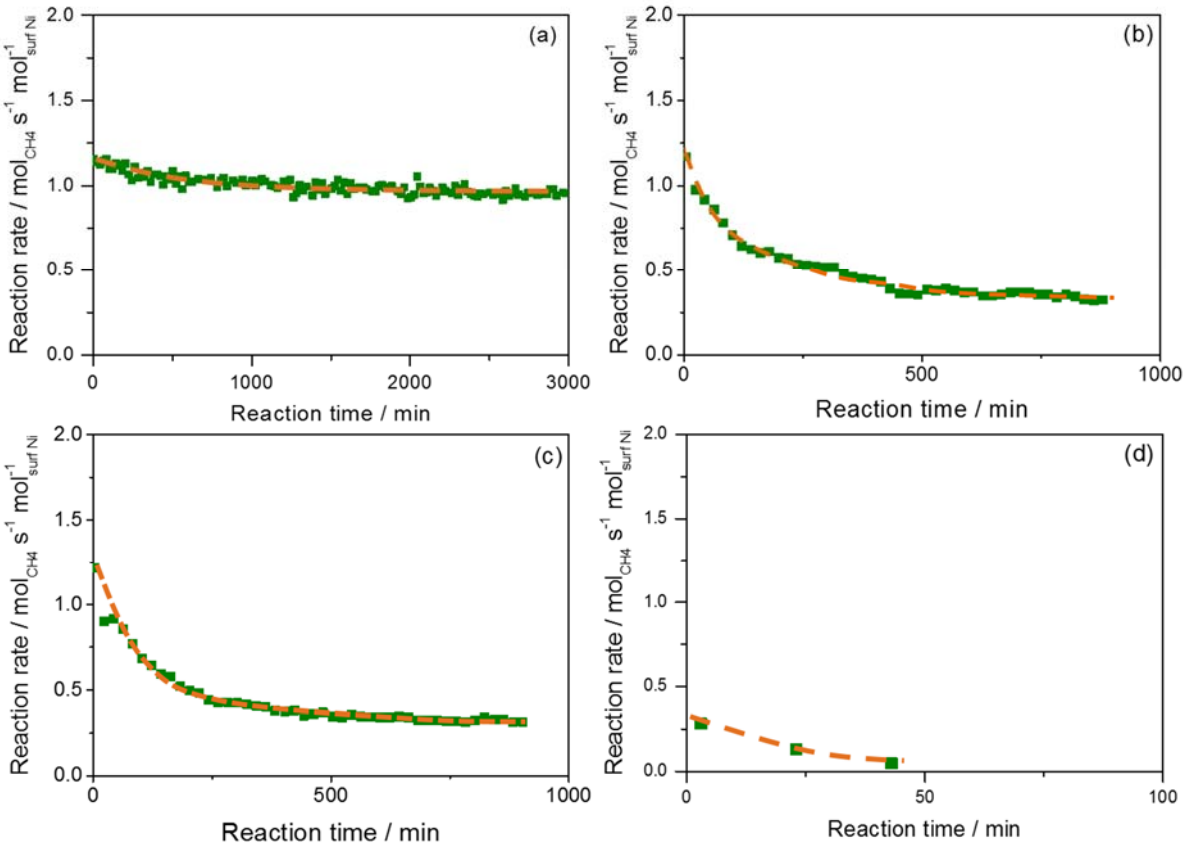

Figure 6. Reaction rate of CH_4 over (a) 1 wt.% Ni/ZrO_2, (b) 2 wt.% Ni/ZrO_2 (c) 5 wt.% Ni/ZrO_2 and (d) 1 wt.% Ni/SiO_2 at 873 K during DRM reaction.

The concentrations of coke on the spent Ni/ZrO_2 catalysts were compared after 900 min reaction. As shown in Table 3, the 1 wt.% Ni/ZrO_2 showed only a small amount of coke deposited (1.2 mol_C $mol_{surf\ Ni}^{-1}$), while the catalysts with 2 and 5 wt.% Ni on ZrO_2 suffered from a fast coke accumulation during DRM, generating 60 and 48 mol_C $mol_{surf\ Ni}^{-1}$, respectively. These results were consistent with our aforementioned hypothesis that Ni/ZrO_2 with a metal particle size of around 1 nm could kinetically inhibit the formation of coke and that the rate of coke deposition would increase with larger Ni particle size. The stable activity of 1 wt.% Ni/ZrO_2 during DRM is also reflected in the constant concentration of coke deposited on the catalysts shown in Figure 7. The concentration of carbon on the spent catalysts remained constant after 20 mins over 1 wt% Ni/ZrO_2, confirming efficient coke removal via reaction with surface oxygen species.

Table 3. Concentration of coke deposited over 1 wt.% Ni/ZrO_2, 2 wt.% Ni/ZrO_2 and 5 wt.% Ni/ZrO_2 at 873 K after 900 mins of DRM reaction.

Catalyst	1 wt.% Ni/ZrO_2	2 wt.% Ni/ZrO_2	5 wt.% Ni/ZrO_2
Amount of coke ($mol_C\ mol_{surf\ Ni}^{-1}$)	1.2	60	48

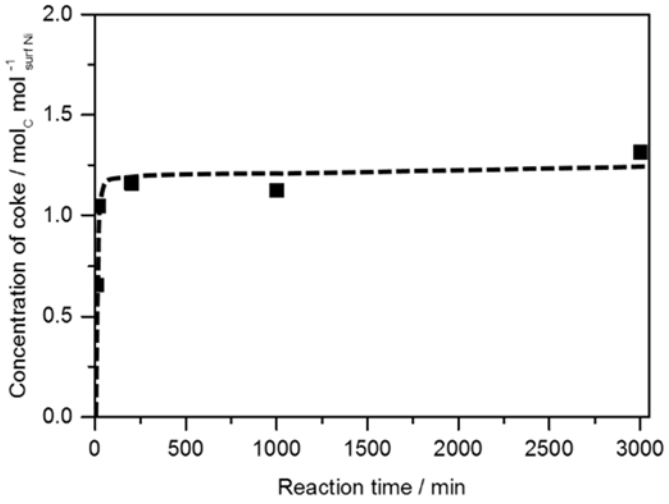

Figure 7. Concentration of coke accumulated on 1 wt.% Ni/ZrO_2 during DRM reaction at 873 K.

It is interesting to note that H_2O formation deactivated slower than H_2 formation during DRM; H_2 and H_2O yields with TOS during DRM are shown in Figure 8a-c. All the three Ni/ZrO_2 catalysts showed a stable H_2O yield within the reaction time, but a clear decrease of H_2 yield, especially on 2 wt.% and 5 wt.% catalysts were observed. For example, the H_2 yield underwent a 56% decrease after 900 min TOS on the 5 wt.% Ni/ZrO_2 catalyst, while H_2O yield decreased only 18%. In particular, when removing the surface coke via reverse Boudouard reaction under CO_2, the H_2 formation activity was largely recovered, while the H_2O formation was unaffected (Fig. S2). These results indicate two different pathways and active sites for H_2O and H_2 formation. The Ni sites catalyzing H_2 formation on Ni/ZrO_2 are easier blocked by carbon. We hypothesize that on larger particles these sites are not located at the perimeter. Water formation, on the other hand, was concluded to occur mostly on sites that are hardly affected by coke, i.e., at Ni at the perimeter. Thus, the evolution pattern of H_2O yield with TOS can be explained by the decrease of the concentration of sites for CO_2 activation on the non-

perimeter Ni (Eq. 14a) in the initial stage and a stable formation of H_2O (supply of O via CO_2 activation) on the Ni-ZrO_2 perimeter during the entire DRM reaction process (Eq. 14b).

$$H^* + O^* \rightleftharpoons OH^* + *\ ; \qquad OH^* + H^* \rightleftharpoons H_2O + 2\,*$$

(on non-perimeter Ni (minority))..(14a)

(on perimeter Ni (majority))……..(14b)

The evolution of the yields of H_2O and H_2 formation with time on stream allows to monitor catalyst deactivation for different active sites and reaction pathways.

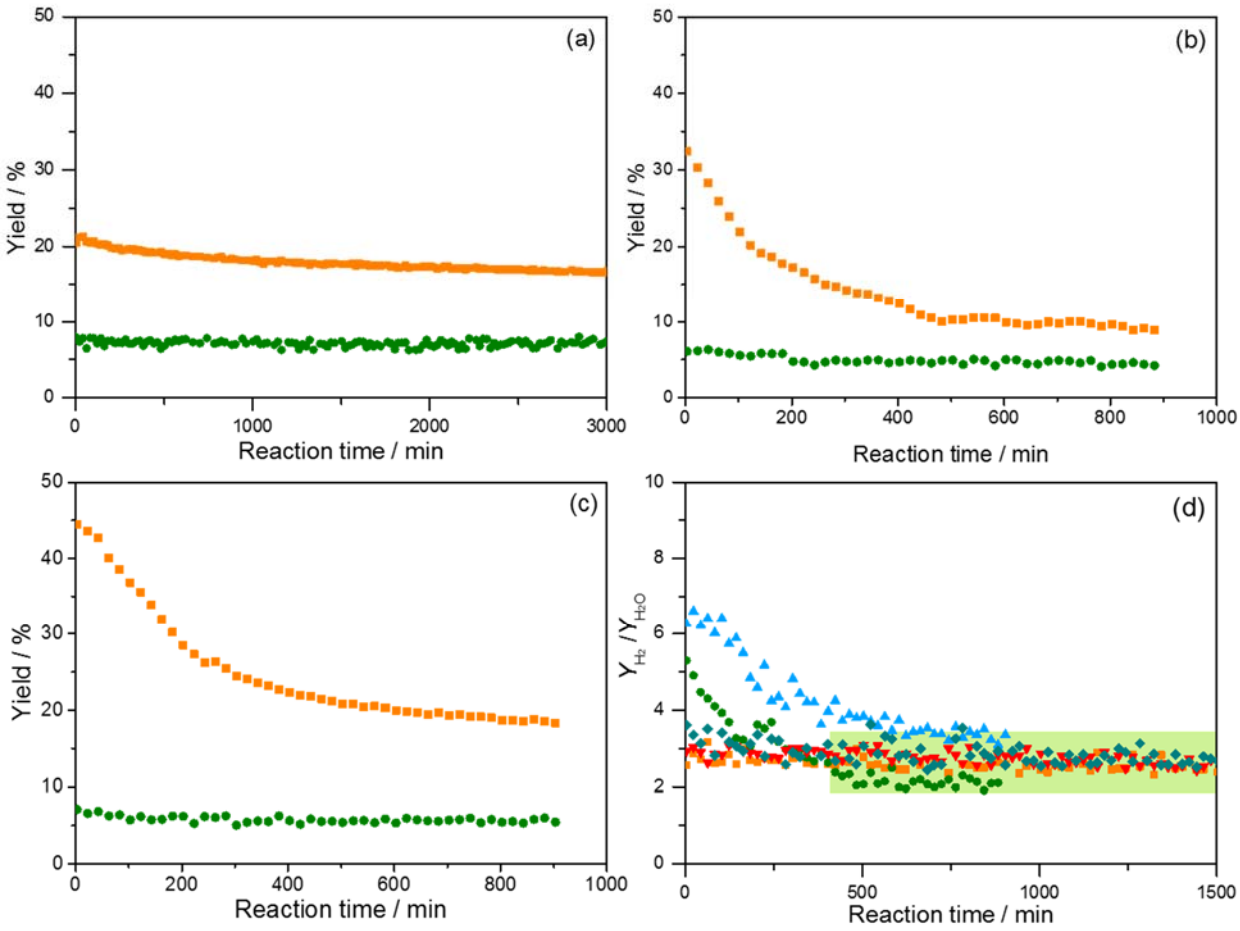

Figure 8. Yields of H_2 (■) and H_2O (■) formation over (a) 1 wt.% Ni/ZrO_2, (b) 2 wt.% Ni/ZrO_2, (c) 5 wt.% Ni/ZrO_2 at 873 K during DRM reaction and (d) Ratios of H_2 to H_2O yield over (■) 1 wt.% Ni/ZrO_2, (●) 2 wt.% Ni/ZrO_2, (▲) 5 wt.% Ni/ZrO_2, (▼) Zr6Ni3imp and (◆) Zr82Ni3imp at 873 K during DRM reaction. The green horizontal bar in (d) represents the interval of Y_{H_2}/Y_{H_2O} values under steady state.

The ratio between H_2 and H_2O yields over Ni/ZrO_2 at 873 K are shown as function of time on stream in Figure **9**8d. The Ni/ZrO_2 catalysts had different initial Y_{H_2}/Y_{H_2O} values, e.g., 2.6 for 1 wt.% Ni/ZrO_2, 5.3 for 2 wt.% Ni/ZrO_2 and 6.3 for 5 wt.% Ni/ZrO_2, which, however, approached and stabilized at the same level (2.5 ± 0.5) after some time on stream (Fig. 8d). This is further shown on two stable Ni/ZrO_2 catalysts (Zr6Ni3imp (2.7 wt.% Ni/ZrO_2) and Zr82Ni3imp (3 wt.% Ni/ZrO_2), Fig. S3-4) synthesized by impregnation with the concomitant addition of $NaHCO_3$ published previously [50, 51]. Although the Ni particle size of these two catalysts were relatively large (20 nm) as estimated by XRD and CO chemisorption, XPS suggested higher surface Ni fraction. The localized Na_2O on and around Ni provided an extended ZrO_2-Na_2O-Ni interface which increased the ability of CO_2 adsorption and activation, facilitating coke removal. [50, 51]. It is noteworthy that all stable catalysts (1 wt.% Ni/ZrO_2, Zr6Ni3imp and Zr82Ni3imp) showed an initial Y_{H_2O}/Y_{H_2} value close to 0.4 (Fig. 9a). This is not driven by equilibrium of reverse water gas shift (RWGS), because none of the catalysts reached equilibrium of RWGS (Fig. S5). Although most results published on dry reforming were under the equilibrium of water gas shift, some works were carried out far from this equilibrium [35, 54-57]. The low catalyst loading and consequently the low conversion level of methane made our reaction away from RWGS equilibrium. Theses catalysts reached Y_{H_2O}/Y_{H_2} ratio of 0.4 at different approach to RWGS equilibrium (Fig. 9b), showing the independence of the Y_{H_2O}/Y_{H_2} ratio on RWGS under the DRM reaction conditions used.

Here, we assign this number (Y_{H_2O}/Y_{H_2} = 0.4), based on the results from our previous work, to the quantitative selectivity ratio between H_2O and H_2 formed on the perimeter Ni, because the non-perimeter Ni (n-per Ni) was completely covered by coke after deactivating to a stable level [17]. Ni/ZrO_2 catalysts with an initial Y_{H_2O}/Y_{H_2} value close to 0.4 showed much more stable DRM activity compared to DRM on Ni/ZrO_2 catalysts with lower initial Y_{H_2O}/Y_{H_2}. The 1 wt.% Ni/SiO_2 showed the lowest initial Y_{H_2O}/Y_{H_2} ratio and the strongest deactivation. Especially, unlike Ni/ZrO_2, the Y_{H_2O}/Y_{H_2} value of 1 wt.% Ni/SiO_2 was almost unchanged, even after it lost 85% activity after 50 min TOS. Since SiO_2 is not capable to activate CO_2, all CO_2 was activated on the Ni surface, identical in properties to non-perimeter Ni in Ni/ZrO_2. Therefore, the constant Y_{H_2O}/Y_{H_2} ratio of ~0.13 on 1 wt% Ni/SiO_2 represents the Y_{H_2O}/Y_{H_2} ratio of non-perimeter Ni in the Ni/ZrO_2 catalysts (neglecting subtle modifications in properties by variations of electronic properties of Ni induced by different supports).

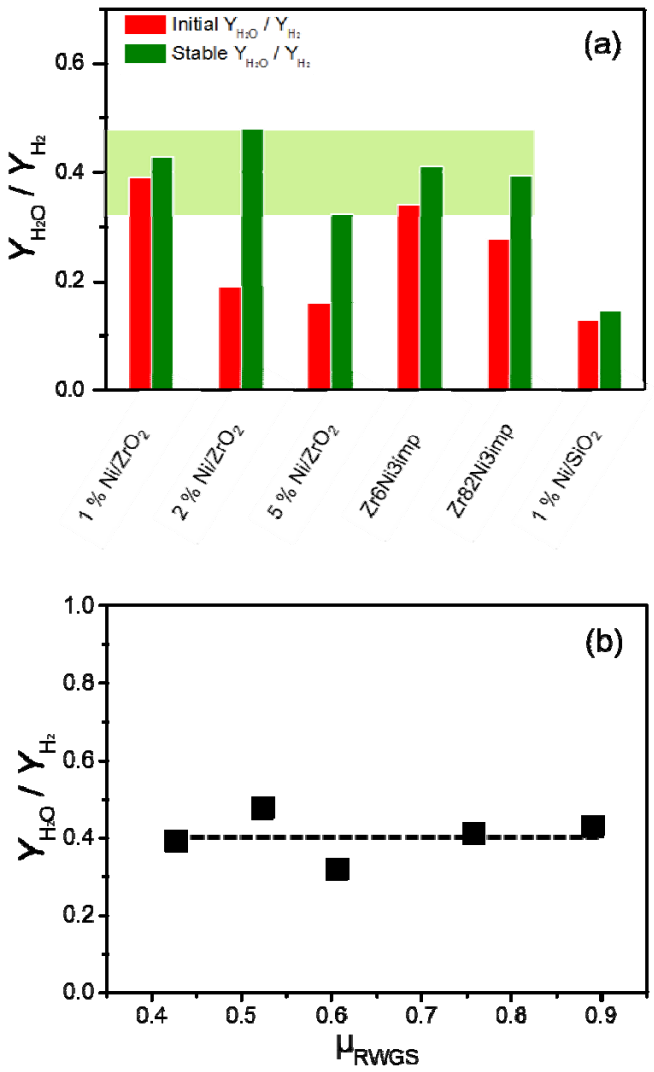

Figure 9. (a) Initial (red) and stable (green) ratios of Y_{H_2O}/Y_{H_2} over Ni/ZrO_2 catalysts and 1 wt.% Ni/SiO_2 at 873 K during DRM reaction. Since 1 wt% Ni/SiO_2 never came to a stable reaction, values were used at 50 min TOS when it had lost 83 % activity. (b) The yield ratio between H_2O and H_2 on stable catalyst or on catalyst deactivated to a stable level as a function of the approach to RWGS equilibrium. The green horizontal bar in (a) represents the interval of Y_{H_2O}/Y_{H_2} values under steady state.

Catalyst deactivation and oxygen availability index (OAI).

Having shown the strong correlation between the stability of Ni and the formation ratio between H_2O and H_2, we analyze, how this ratio affects the Ni catalyst deactivation. As discussed, dry reforming is initiated on Ni via dissociative adsorption of CH_4, forming surface C and H (Eq. 5) (We have not considered the –C-H_x species for simplicity, as they were considered to be reversibly formed intermediates.). In the absence of O, H leaves the surface via formation of H_2 (Eq. 7), while C accumulates and restructures to coke (Eq. 10). With the

accessibility to O, H and C could leave the surface as H_2O (Eq. 8) and CO (Eq. 9), thus, coke formation and deactivation is kinetically reduced.

The quantitative analysis of these elementary reaction steps is shown below. The coke formation rate is given as Equation 15 based on Equation 10.

$$r_{\mathrm{C}} = k_{10} \cdot \theta_c^{\alpha} \qquad (15)$$

in which r_C is the rate of coke formation, θ_c is proportional to the coverage of surface carbon species on Ni. Coke cannot be formed on single isolated surface carbon as it requires coupling between surface carbons. Therefore, a reaction order, α, was introduced in Equation 15 to represent the interaction between carbon atoms. Under steady state reaction, C removal together with coke deposition should balance the C input from methane. Considering that the coke amount formed is only a very small fraction of total converted methane, the C removal as CO approximates the C input from methane (Eq. 16).

$$r_{\mathrm{CH_4}} = r_9 = k_9 \cdot \theta_C \cdot \theta_{\mathrm{O}} \qquad (16)$$

θ_{O} is the coverage of surface oxygen species supplied by the activation of CO_2 molecule. Rearrangement of Equations 15 and 16 leads to the following expression

$$r_{\mathrm{C}} = k_{10} \cdot k_9^{-\alpha} \cdot r_{\mathrm{CH_4}}^{\alpha} \cdot \theta_{\mathrm{O}}^{-\alpha} \qquad (17)$$

It is seen from Equation 17 that the coke formation rate is strongly negatively correlated with the O coverage on Ni. The coverage of O is hardly measurable in the reaction, however, it can be represented by the ratio between H_2O and H_2.

To express the coverage of O, the equilibrium of H_2 and H_2O with surface H, OH and O are expressed as Equation 18 and 19.

$$P_{\mathrm{H_2}} = K_7 \cdot \theta_{\mathrm{H}}^2 \cdot \theta_*^{-2} \qquad (18)$$

$$\theta_{\mathrm{OH}} \cdot \theta_* = K_{8\mathrm{a}} \cdot \theta_{\mathrm{H}} \cdot \theta_{\mathrm{O}} \qquad (19a)$$

$$P_{\mathrm{H_2O}} = K_{8\mathrm{b}} \cdot \theta_{\mathrm{H}} \cdot \theta_{\mathrm{OH}} \cdot \theta_*^{-2} \qquad (19b)$$

The θ_* is the fraction of empty sites on Ni surface. Then, θ_{O} can be obtained from equations 18-19:

$$\theta_{\mathrm{O}} = \frac{K_7}{K_{8\mathrm{a}} K_{8\mathrm{b}}} \cdot \frac{P_{\mathrm{H_2O}}}{P_{\mathrm{H_2}}} \cdot \theta_* \qquad (20a)$$

$$\theta_{\mathrm{O}}^{-1} = \frac{K_{8a}K_{8b}}{K_7} \cdot \frac{P_{\mathrm{H_2}}}{P_{\mathrm{H_2O}}} \cdot \theta_*^{-1} \qquad (20b)$$

Noticeable from Equation 20b, the ratio between H_2O and H_2 (P_{H_2O}/P_{H_2}) is proportional to the O coverage (θ_O). Actually, the ratio of H_2O to H_2 in pressure equals to their ratio in yield ($P_{H_2O}/P_{H_2} = Y_{H_2O}/Y_{H_2}$). Here we define these two ratios as the surface oxygen availability index (OAI, Eq. 21), representing the abundance of O on the Ni surface. With this OAI, coke formation rate (Eq. 17) is expressed as:

$$\mathrm{OAI} = \frac{P_{\mathrm{H_2O}}}{P_{\mathrm{H_2}}} = \frac{Y_{\mathrm{H_2O}}}{Y_{\mathrm{H_2}}} \qquad (21)$$

$$r_{\mathrm{C}} = k_{10} \cdot \left(\frac{K_{8a}K_{8b}}{K_7 \cdot k_9}\right)^{\alpha} \cdot r_{\mathrm{CH_4}}^{\alpha} \cdot \theta_*^{-\alpha} \cdot (\mathrm{OAI})^{-\alpha} \qquad (22)$$

It is seen from Equation 22 that coke formation rate is inversely correlated with the OAI. Thus, we can use this value to evaluate the deactivation of ZrO_2 supported nickel catalysts in DRM. The relation between initial deactivation rate and initial OAI on Ni/ZrO_2 and Ni/SiO_2 catalysts are plotted in Figure 10, in which the deactivation rate of DRM catalysts is defined as the loss of active surface Ni per unit time:

$$\text{Deactivation rate} = \frac{\mathrm{d}(C_{\text{surf Ni}})}{\mathrm{d}(\mathrm{TOS})} \qquad (23)$$

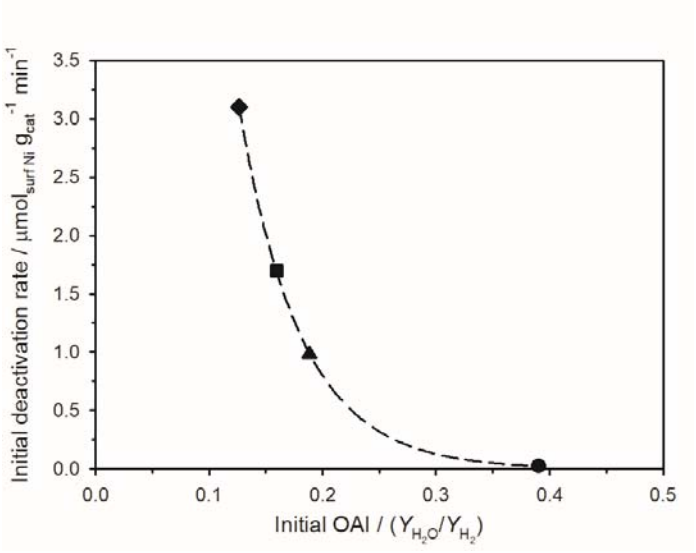

Figure 10. Initial deactivation rate as a function of initial OAI (surface oxygen availability index) over 1 wt.% Ni/ZrO_2 (●), 2 wt.% Ni/ZrO_2 (▲), 5 wt.% Ni/ZrO_2 (■), and 1 wt.% Ni/SiO_2 (◆) at 873 K during DRM reaction. Deactivation rate is shown as the rate of the loss of active surface Ni.

It is remarkable that the deactivation rate decreased with the OAI value (Fig. 10). When OAI reaches 0.4 or above, the high O abundance on Ni provides efficient removal of C via CO, reducing coke formation and making catalyst stable. This is also supported by the result in a recent report of Weifeng et al., in which Ni/MgO-ZrO_2 having OAI above 0.4 showed stable activity in DRM under the same temperature to ours [12]. For OAI below 0.4, insufficient C removal strongly deactivates the catalyst. This correlation indicates the importance of perimeter Ni for the catalyst stability in the DRM reactions, which increases the O abundance on Ni surface by delivering surface oxygen to surface carbons, preventing coke formation.

The difference in O accessibility for perimeter Ni and non-perimeter Ni and consequently the different OAI values on them allow in turn to determine the ratio between the concentration of perimeter and non-perimeter Ni atoms. The OAI value on the perimeter Ni is 0.40 as we have shown on stable Ni/ZrO_2 catalysts and unstable Ni/ZrO_2 catalyst after deactivation to a constant rate. The OAI value on non-perimeter Ni is 0.13, which is estimated from the value of Ni/SiO_2 catalysts. The initial OAI value of 0.17 on 5 wt.% Ni/ZrO_2 catalyst indicates the fraction of perimeter Ni in all surface Ni was 12%. Accounting for the surface Ni concentration of 336 μmol g^{-1} on fresh 5 wt.% Ni/ZrO_2 catalyst, the perimeter and non-perimeter Ni were therefore calculated to be 41 and 295 μmol g^{-1}, respectively. Following this method, the concentrations of not deactivated perimeter Ni and non-perimeter Ni during the deactivation of Ni/ZrO_2 catalysts can be estimated. For example, 5 wt.% Ni/ZrO_2, after TOS of 200 min, deactivated and remained only 41% of its initial activity, corresponding to 137 μmol g^{-1} Ni remained active on the surface. Its OAI value increased to 0.22, meaning a perimeter Ni fraction of 34% in the remaining 137 μmol g^{-1} Ni, which points to 46 μmol g^{-1} perimeter Ni and 90 μmol g^{-1} non-perimeter Ni remained active. The concentrations of different Ni surface species during Ni/ZrO_2 deactivation are shown in Figure 11, plotted as the evolution of a particular type of Ni with the overall decrease of accessible surface Ni. It is seen that on all the three Ni/ZrO_2, the concentration of perimeter Ni was almost unchanged, regardless of the drop of total active surface Ni. In contrast, non-perimeter Ni concentration declined continuously, with a slope of 1.0 - 1.1 on all the three catalysts. The slope close to unity indicates that the loss of Ni during deactivation is the loss of non-perimeter Ni. In other word, the Ni sites blocked by coke were only non-perimeter Ni and the perimeter Ni remained free of coke blockage. Therefore, the OAI value of a fresh Ni/ZrO_2 catalyst allows to predict its deactivation rate as well as its stabilized activity.

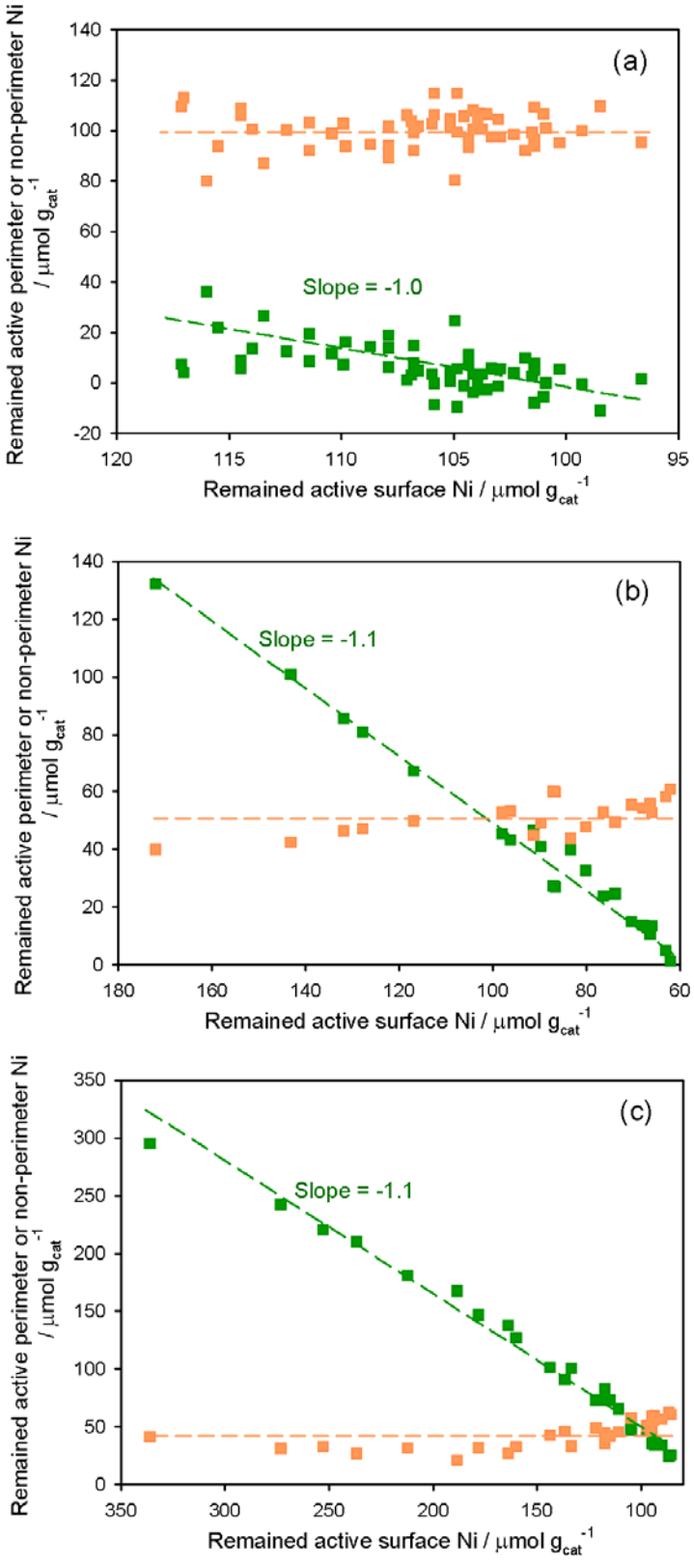

Figure 11. The concentration of perimeter Ni (■) and non-perimeter Ni (■) that remained active during the deactivation of (a) 1 wt% Ni/ZrO_2, (b) 2 wt.% Ni/ZrO_2 and (c) 5 wt.% Ni/ZrO_2 at 873 K during DRM reactions. The deactivation of catalyst is shown as the concentration of surface Ni remained active.

CONCLUSION

The synthesis method reported here sterically separates Ni precursors into molecular capsules to prepare monodispersed ZrO_2 supported Ni particles of approximately 1.0 nm diameter as long as the loading does not exceed 1 wt.% Ni. For such Ni particles all accessible Ni is located at the perimeter interface. All Ni is not only accessible from the gas phase, but also sufficiently close to the perimeter of the support to have access to labile surface O provided by CO_2 activation at the interface of Ni and ZrO_2. This leads to a fast removal of surface C via CO formation, to a low rate of coke formation and to an outstanding catalyst stability. Larger Ni particles ($d > 1$ nm) contain a fraction of non-perimeter Ni, which have low accessibility to oxygen and generate coke with substantial rates, leading to at least partial deactivation.

The kinetic analysis showed that this process was inversely linked to the availability of oxygen, characterized by the ratio of the yields of H_2O and H_2 formation, which has been named oxygen availability index (OAI). Using a catalyst that was only producing oxygen via dissociation of CO_2 on the metal and one catalyst with only the perimeter zone active, the relative fractions for deactivating and non-deactivating zones were estimated. For Ni/ZrO_2 the perimeter Ni at $Ni\text{-}ZrO_2$ interface had an OAI value of 0.4 and hardly deactivates, while non-perimeter Ni had an OAI of 0.13, deactivating fast by coke formation. All stable Ni/ZrO_2 catalysts had OAI value of approximately 0.4, while unstable Ni/ZrO_2 gradually increased to that value as the catalysis stabilized. This shows that for the system Ni/ZrO_2 only Ni atoms at the perimeter were stable catalytic sites in dry methane reforming.

Concluding it should be emphasized that the OAI allows to classify stable and unstable metal surface atoms. The individual rates and in consequence the OAI will depend on a particular metal and rate at which the support provides labile oxygen atoms. Thus, the rate and the stability will be higher on metals that are better in dissociating CO_2 or able to retain oxygen [12] and will be less stable for systems that dissociate CH_4 with a high rate and have a low tendency to retain oxygen. Similarly, the ability of activating CO_2 and the chemical potential of the oxygen produced with oxides other than ZrO_2 may change the numeric values of OAI. The OAI value, however, gives a clear design criterion for future stable dry reforming catalysts.

ACKNOWLEDGMENT

This work was financially supported by the Deutsche Forschungsgemeinschaft (LE 1187/12-1) under project ERA Chem and the BMBF under the project ZeitKatMat and MatDynamics. A. H. thanks the support from ERA Chem and the National Research, Development and Innovation Office of Hungary (NN107170). The X-Ray absorption experiments were performed on the SuperXAS beamline at the Swiss Light Source, Paul Scherrer Institut, Villigen, Switzerland. The authors gratefully acknowledge the beamline scientists Maarten Nachtegaal and Olga Safonova for their help during the beamtime.

References

[1] M.C.J. Bradford, M.A. Vannice, Catal. Rev.-Sci. Eng., 41 (1999) 1-42.

[2] M.-S. Fan, A.Z. Abdullah, S. Bhatia, Chemcatchem, 1 (2009) 192-208.

[3] J.A. Lercher, J.H. Bitter, W. Hally, W. Niessen, K. Seshan, Studies in Surface Science and Catalysis, Elsevier, 1996, pp. 463-472.

[4] J.H. Bitter, W. Hally, K. Seshan, J.G. vanOmmen, J.A. Lercher, Catalysis Today, 29 (1996) 349-353.

[5] J.H. Bitter, K. Seshan, J.A. Lercher, J. Catal., 171 (1997) 279-286.

[6] J.H. Bitter, K. Seshan, J.A. Lercher, J. Catal., 176 (1998) 93-101.

[7] A. Kambolis, H. Matralis, A. Trovarelli, C. Papadopoulou, Appl. Catal. A: Gen., 377 (2010) 16-26.

[8] M. Khajenoori, M. Rezaei, F. Meshkani, Chem Eng Technol, 37 (2014) 957-963.

[9] J.A. Montoya, E. Romero-Pascual, C. Gimon, P. Del Angel, A. Monzon, Catalysis Today, 63 (2000) 71-85.

[10] J. Newnham, K. Mantri, M.H. Amin, J. Tardio, S.K. Bhargava, International Journal of Hydrogen Energy, 37 (2012) 1454-1464.

[11] B.Q. Xu, J.M. Wei, Y.T. Yu, Y. Li, J.L. Li, Q.M. Zhu, Journal of Physical Chemistry B, 107 (2003) 5203-5207.

[12] W. Tu, M. Ghoussoub, C.V. Singh, Y.C. Chin, J Am Chem Soc, 139 (2017) 6928-6945.

[13] S.M. Kim, P.M. Abdala, T. Margossian, D. Hosseini, L. Foppa, A. Armutlulu, W. van Beek, A. Comas-Vives, C. Coperet, C. Muller, J Am Chem Soc, 139 (2017) 1937-1949.

[14] M. Steib, Y. Lou, A. Jentys, J.A. Lercher, Chemcatchem, DOI: 10.1002/cctc.201700686.

[15] T. Osaki, T. Mori, J. Catal., 204 (2001) 89-97.

[16] J.H. Bitter, K. Seshan, J.A. Lercher, J. Catal., 183 (1999) 336-343.

[17] K. Nagaoka, K. Seshan, K. Aika, J.A. Lercher, J. Catal., 197 (2001) 34-42.

[18] K. Seshan, J.H. Bitter, J.A. Lercher, Recent Advances in Basic and Applied Aspects of Industrial Catalysis, 1998, pp. 187-191.

[19] W. Hally, J.H. Bitter, K. Seshan, J.A. Lercher, J.R.H. Ross, Studies in Surface Science and Catalysis, Elsevier, 1994, pp. 167-173.

[20] C.T. Campbell, C.H.F. Peden, Science, 309 (2005) 713-714.

[21] D. Baudouin, K.C. Szeto, P. Laurent, A. De Mallmann, B. Fenet, L. Veyre, U. Rodemerck, C. Copere, C. Thieuleux, J Am Chem Soc, 134 (2012) 20624-20627.

[22] T. Xie, L.Y. Shi, J.P. Zhang, D.S. Zhang, Chem Commun, 50 (2014) 7250-7253.

[23] F. Mirzaei, M. Rezaei, F. Meshkani, Chem Eng Technol, 37 (2014) 973-978.

[24] J.W. Han, C. Kim, J.S. Park, H. Lee, Chemsuschem, 7 (2014) 451-456.

[25] T.D. Gould, A. Izar, A.W. Weimer, J.L. Falconer, J.W. Medlin, Acs Catal, 4 (2014) 2714-2717.

[26] T. Wu, W.Y. Cai, P. Zhang, X.F. Song, L. Gao, Rsc Adv, 3 (2013) 23976-23979.

[27] Z. Liu, J. Zhou, K. Cao, W. Yang, H. Gao, Y. Wang, H. Li, Applied Catalysis B-Environmental, 125 (2012) 324-330.

[28] D. Halliche, O. Cherifi, A. Auroux, Thermochim Acta, 434 (2005) 125-131.

[29] P. Frontera, A. Macario, A. Aloise, F. Crea, P.L. Antonucci, J.B. Nagy, F. Frusteri, G. Giordano, Catalysis Today, 179 (2012) 52-60.

[30] S. Kawi, Y. Kathiraser, J. Ni, U. Oemar, Z.W. Li, E.T. Saw, Chemsuschem, 8 (2015) 3556-3575.

[31] Z.C. Liu, J. Zhou, K. Cao, W.M. Yang, H.X. Gao, Y.D. Wang, H.X. Li, Applied Catalysis B-Environmental, 125 (2012) 324-330.

[32] N. Wang, Z.X. Xu, J. Deng, K. Shen, X.P. Yu, W.Z. Qian, W. Chu, F. Wei, Chemcatchem, 6 (2014) 1470-1480.

[33] N. Wang, K. Shen, L.H. Huang, X.P. Yu, W.Z. Qian, W. Chu, Acs Catal, 3 (2013) 1638-1651.

[34] C.J. Chen, X.G. Wang, L. ZHang, X.J. Zou, W.Z. Ding, X.G. Lu, Catal Commun, 94 (2017) 38-41.

[35] T. Margossian, K. Larmier, S.M. Kim, F. Krumeich, A. Fedorov, P. Chen, C.R. Muller, C. Coperet, J Am Chem Soc, 139 (2017) 6919-6927.

[36] T. Gerkensmeier, W. Iwanek, C. Agena, R. Fröhlich, S. Kotila, C. Näther, J. Mattay, European Journal of Organic Chemistry, 1999 (1999) 2257-2262.

[37] R.M. McKinlay, P.K. Thallapally, G.W.V. Cave, J.L. Atwood, Angew. Chem. Int. Ed., 44 (2005) 5733-5736.

[38] R.M. McKinlay, G.W.V. Cave, J.L. Atwood, P Natl Acad Sci USA, 102 (2005) 5944-5948.

[39] J.L. Atwood, E.K. Brechin, S.J. Dalgarno, R. Inglis, L.F. Jones, A. Mossine, M.J. Paterson, N.P. Power, S.J. Teat, Chem Commun (Camb), 46 (2010) 3484-3486.

[40] H. Kumari, A.V. Mossine, S.R. Kline, C.L. Dennis, D.A. Fowler, S.J. Teat, C.L. Barnes, C.A. Deakyne, J.L. Atwood, Angew. Chem. Int. Ed., 51 (2012) 1452-1454.

[41] S.J. Dalgarno, N.P. Power, J.L. Atwood, Coordin Chem Rev, 252 (2008) 825-841.

[42] L.R. MacGillivray, J.L. Atwood, Nature, 389 (1997) 469-472.

[43] Q. Zhang, K. Tiefenbacher, J Am Chem Soc, 135 (2013) 16213-16219.

[44] C. Pan, K. Pelzer, K. Philippot, B. Chaudret, F. Dassenoy, P. Lecante, M.J. Casanove, J Am Chem Soc, 123 (2001) 7584-7593.

[45] O. Muller, D. Lutzenkirchen-Hecht, R. Frahm, Rev Sci Instrum, 86 (2015).

[46] B. Ravel, M. Newville, J Synchrotron Radiat, 12 (2005) 537-541.

[47] J.J. Rehr, J.J. Kas, F.D. Vila, M.P. Prange, K. Jorissen, Phys Chem Chem Phys, 12 (2010) 5503-5513.

[48] M.C. Letzel, C. Agena, J. Mattay, J Mass Spectrom, 37 (2002) 63-68.

[49] Q. Zhang, K. Tiefenbacher, Nat Chem, 7 (2015) 197-202.

[50] M. Nemeth, D. Sranko, J. Karolyi, F. Somodi, Z. Schay, G. Safran, I. Sajo, A. Horvath, Catal Sci Technol, (2017).

[51] M. Nemeth, Z. Schay, D. Sranko, J. Karolyi, G. Safran, I. Sajo, A. Horvath, Appl. Catal. A: Gen., 504 (2015) 608-620.

[52] S. Cai, C. Seu, Z. Kovacs, A.D. Sherry, Y. Chen, J Am Chem Soc, 128 (2006) 13474-13478.

[53] M. Boualleg, J.-M. Basset, J.-P. Candy, P. Delichere, K. Pelzer, L. Veyre, C. Thieuleux, Chemistry of Materials, 21 (2009) 775-+.

[54] A. M. Gaddalla, M. E. Sommer, Chem Eng Sci, 44 (1989) 2825-2829.

[55] H.D. Gesser, N.R. Hunter, A.N. Shigapov, V. Januati, Energ Fuel, 8 (1994) 1123-1125.

[56] M.C.J. Bradford, M.A. Vannice, Appl. Catal. A: Gen., 142 (1996) 97-122.

[57] J.T. Richardson, S.A. Paripatyadar, Appl Catal, 61 (1990) 293-309.